Accuracy verification of a 2D adaptive mesh refinement method using backward facing step flows of low Reynolds numbers

†Zhenquan Li[1], and Miao Li[2]

[1]School of Computing and Mathematics, Charles Sturt University, Australia.
[2]CSU Engineering, Charles Sturt University, Australia.

*Presenting author: jali@csu.edu.au
†Corresponding author: jali@csu.edu.au

Abstract

Identifying accurate centers of vortices of fluid flow is one of the accuracy measures for computational methods. After verifying the accuracy of the 2D adaptive mesh refinement (AMR) method by the benchmarks of 2D lid-driven cavity flows, this paper shows the accuracy verification by the benchmarks of 2D backward facing step flows. The AMR method refines a mesh using the numerical solutions of the Navier-Stokes equations calculated on the mesh by an open source software Navier2D which implemented a vertex centered finite volume method (FVM) using the median dual mesh to form control volumes about each vertex. The accuracy of the refined meshes is shown by the centers of vortices given in the benchmarks being held within the twice refined cells. The accuracy is also shown by the comparison between vortex center locations calculated from the linearly interpolated numerical solutions and those obtained in the benchmark. The AMR method is proposed based on the qualitative theory of differential equations, and it can be applied to refine a mesh as many times as required and used to seek accurate numerical solutions of the mathematical models including the continuity equation for incompressible fluid or steady-state fluid flow with low computational cost.

Keywords: adaptive mesh refinement, finite volume method, backward facing step flow

Introduction

The AMR is a computational approach to increase the accuracy of numerical solutions of differential equations with low computational cost. A big number of papers on AMRs and their applications have been published [1]. Some common AMR methods take local truncation errors as a refinement criterion (e.g. Almgren et al. [2]). Other common AMR methods include h-refinement (e.g. Lohner [3]), p-refinement (e.g. Bell et al. [4]) or r-refinement (e.g. Miller et al. [5]), and different combinations of the above (e.g. Capon et al. [6]). These AMR methods aim to obtain a balance between the accuracy and the computational cost in finding numerical solutions of differential equations.

We introduced AMR methods for calculating accurate 2D (Li [7]) and 3D numerical velocity fields (Li [8]) based on a theory derived from Theorem 1.14 in the book by Ye et al. [9]. The theorem states that a 2D vector field has no one sided limit cycles if it satisfies the continuity equation. In other words, all trajectories of a vector field are closed curves in bounded domains if the vector field satisfies the continuity equation. A vector field which satisfies continuity equation is called divergence free field. The benchmarks (e.g. Erturk et al. [10]) confirm the theorem numerically. The AMR method refines a mesh based on the velocity fields calculated numerically on it. The refinement can be performed as many times as required. The more the

refinements, the less the area on which the linearly interpolated velocity field is not equivalent to a divergence free vector field is.

Locating singular points, and drawing accurate asymptotic lines (planes) and closed streamlines of a calculated velocity field are commonly used to measure the accuracy of computational methods. We demonstrated the accuracy of the AMR methods using examples of analytical velocity fields by comparing the exact results from the analytical velocity fields with the corresponding results from the numerical velocity fields that take vectors of the analytical velocity fields at nodes of the meshes: the singular points and asymptotic lines for 2D [11]; the singular points and asymptotic plane for 3D [12]; and closed streamlines (Li [11]-[12]). We also demonstrated the accuracy of the 2D AMR method using numerical velocity fields of 2D steady incompressible lid-driven cavity flows (Lal et al. [13]). We obtained numerical velocity fields of the Navier-Stokes equations with the boundary conditions using a second order collocated FVM (GSFV) with a splitting method for time discretization (Faure et al. [14]). We applied the AMR method once to the initial meshes based on the numerical velocity fields calculated by GSFV on them, and estimated the singular point locations using the centers of refined cells in the corresponding vortex regions. The estimated locations are accurate by comparing with the corresponding benchmarks.

Mesh refinement is necessary for calculating accurate numerical solutions since different levels of vortices requires different densities of mesh nodes (Li [15]). The same conclusion was obtained by Armaly et al. [16]. We conducted a study starting from relatively coarse initial meshes and demonstrating that the centers of vortices were held within the refined cells of once refined meshes (Li et al. [17]). We also verified the accuracy of the AMR method by applying the method twice to the initial meshes. Li et al. [1] applied the AMR method twice to the initial meshes and the twice refined meshes show that centres of the vortices are held within the twice refined cells. Li [18] considered flow past a square cylinder over symmetrical domain but the streamlines drawn on the initial mesh are not symmetrical. The symmetry of streamlines on the refined meshes are improved significantly after applying the AMR method once on the initial meshes.

This paper demonstrates the accuracy of the 2D AMR method proposed by Li [7] using the benchmarks for 2D backward facing step flows. The backward facing step flows have features of separation, reattachment, recirculation and shear layers in the flow region. We conduct study with constant boundary and initial conditions at the inlet channel and apply the AMR method twice to the initial meshes. We compare the profiles of the exact horizontal component of the velocity field and the profiles obtained numerically after the flow is well developed at the step [19]. Finally we show the differences between calculated locations of all detachment, reattachment and centres of vortices and the corresponding benchmarks [19].

Governing equations

This paper considers the 2D incompressible or steady backward facing step flow. The governing equations are as follows:

$$\nabla \cdot \boldsymbol{V} = 0$$

$$\frac{\partial \boldsymbol{V}}{\partial t} + \boldsymbol{V} \cdot \nabla \boldsymbol{V} = \frac{1}{\rho} \nabla P + \nu \nabla^2 \boldsymbol{V}$$

where $\boldsymbol{V} = (u, v)$ is the velocity field, ν is the kinematic viscosity, and P is the pressure. The governing equations are implemented in MATLAB, named Navier2D by Darren Engwirda [20], and it is used to calculate the velocity field $\boldsymbol{V}$ on triangular meshes numerically.

The computational domain is illustrated in the top figure of Figure 1. The height of the step is designated as h. We choose the length of the upstream channel as $250h$ since the initial conditions for both velocity components in this study are constants at the inlet so the u profile can be developed well enough for long channel. The length of the downstream channels of the step is $50h$.

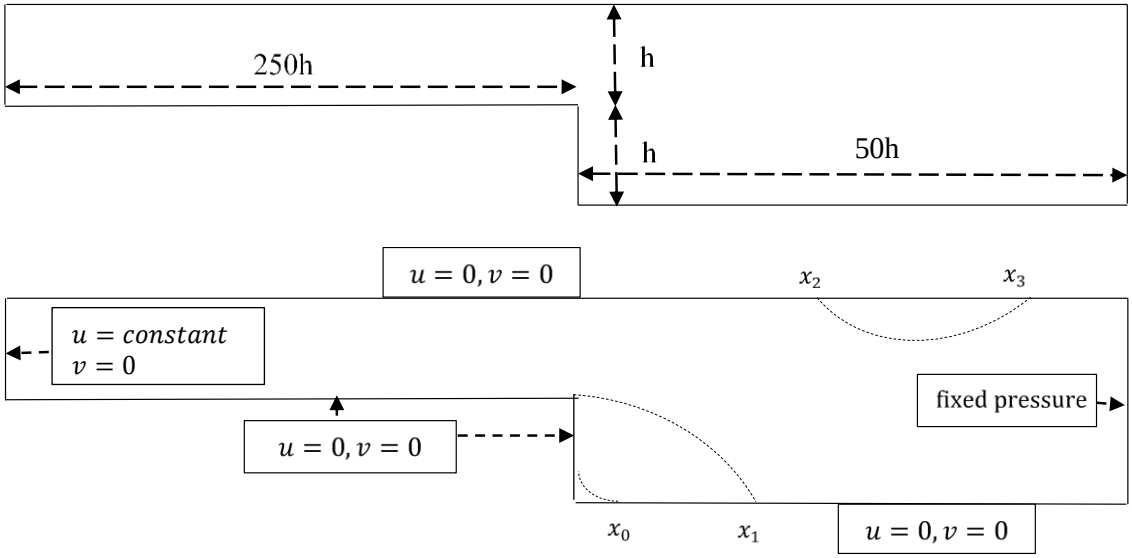

Figure 1. Computational domain and boundary conditions

The boundary conditions and the locations of detachments and reattachment are shown in the bottom figure of Figure 1. The detachments and reattachments y_0, x_0, x_1, x_2 and x_3 are shown in blue, red, cyan, magenta and green dots in the figures in Section 3. The locations of centers of vortices are shown by *. The computational domain is normalized using $h=1$. The outputs in terms of detachments, reattachments and locations of vortices are also normalized and compared with the results in Erturk [19].

Review of AMR Method

This section summarizes the 2D AMR method proposed by Li [7] based on the theory developed from qualitative theory of differential equations [9].

Assume that $\boldsymbol{V}_l = \boldsymbol{AX} + \boldsymbol{b}$ is a vector field on a triangle obtained by linearly interpolating the vectors at the three vertexes of the triangle, where

$$\boldsymbol{A} = \begin{pmatrix} a_{11} & a_{12} \\ a_{21} & a_{22} \end{pmatrix}$$

is a matrix of constants,

$$\boldsymbol{b} = \begin{pmatrix} b'_1 \\ b'_2 \end{pmatrix}$$

is a vector of constants and

$$\boldsymbol{X} = \begin{pmatrix} x_1 \\ x_2 \end{pmatrix}$$

is a vector of spatial variables. The continuity equation for $\boldsymbol{V}_l$ and a steady flow or an incompressible fluid is

$$\nabla \cdot \boldsymbol{V}_l = trace(\boldsymbol{A}) = 0. \tag{1}$$

Let f be a scalar function depending on spatial variables only. Substituting $f\boldsymbol{V}_l$ into the vector field $\boldsymbol{V}$ of the continuity equation $\nabla \cdot \boldsymbol{V} = 0$ obtains a differential equation. Solving the differential equation for f for the four different Jacobian forms of the coefficient matrix $\boldsymbol{A}$ gives the expressions of f as shown in Table 1. In Table 1, $(y_1, y_2)^T = \boldsymbol{V}^{-1}\boldsymbol{X}$ and $(b_1, b_2)^T = \boldsymbol{V}^{-1}\boldsymbol{b}$ where $\boldsymbol{V}$ satisfies $\boldsymbol{AV} = \boldsymbol{VJ}$ and $\boldsymbol{J}$ is one of the Jacobian matrices in Table 1. Vectors $\boldsymbol{V}_l$ and $f\boldsymbol{V}_l$ produce same streamlines if $f \neq 0, \infty$ (refer to Section 2.2 of [11]). The introduction of functions f reduces the number of refined cells in refined meshes dramatically [21].

Table 1. Jacobean matrices and corresponding expressions of f ($C \neq 0$)

Case	Jacobean	f
1	$\begin{pmatrix} r_1 & 0 \\ 0 & r_2 \end{pmatrix} (0 \neq r_1 \neq r_2 \neq 0)$	$\dfrac{C}{\left(y_1 + \dfrac{b_1}{r_1}\right)\left(y_2 + \dfrac{b_2}{r_2}\right)}$
2	$\begin{pmatrix} r_1 & 0 \\ 0 & 0 \end{pmatrix} (r_1 \neq 0)$	$\dfrac{C}{y_1 + \dfrac{b_1}{r_1}}$
3	$\begin{pmatrix} r & 1 \\ 0 & r \end{pmatrix} (r \neq 0)$	$\dfrac{C}{\left(y_2 + \dfrac{b_2}{r}\right)^2}$
4	$\begin{pmatrix} \mu & \lambda \\ -\lambda & \mu \end{pmatrix} (\mu \neq 0, \lambda \neq 0)$	$\dfrac{C}{\left(y_1 + \dfrac{\mu b_1 - \lambda b_2}{\mu^2 + \lambda^2}\right)^2 + \left(y_2 + \dfrac{\lambda b_1 + \mu b_2}{\mu^2 + \lambda^2}\right)^2}$

The conditions (MC)(MC is the abbreviation of mass conservation) are the functions f in Table 1 not equaling zero or infinity at any point on the triangular domains.

We review the algorithm of AMR method for quadrilateral meshes [17]. The algorithm can also be used to a triangular mesh after a subdivision scheme for a triangle is defined. We describe the algorithm of AMR method into two parts:

- cell refinement algorithm - describes how to use the conditions (MC) to refine a quadrilateral cell in a given mesh.
- the algorithm of AMR method.

The AMR is an infinite process. To avoid an infinite refinement of a mesh, we choose a pre-specified threshold number of refinements T based on the accuracy requirements. The algorithm of cell refinement is:

Step 1 Subdivide a quadrilateral cell into two triangles. If $\boldsymbol{V}_l$ satisfies Eq. (1) on both triangles, no refinement for the cell is required. Otherwise, go to Step 2;

Step 2 Apply the conditions (MC) to both of the triangles. If the conditions (MC) are satisfied on both triangles, no refinement for the cell is required. Otherwise, we subdivide the cell into a number of small cells such that the lengths of all sides of the small cells are truly reduced (e.g. connecting the mid-points of opposite sides of a quadrilateral by line segments produces four small quadrilaterals and the lengths of the sides of the four small quadrilaterals are truly reduced).

The algorithm of AMR method is:

Step 1 Evaluate the numerical velocity field for a given initial mesh;

Step 2 Refine all cells of the initial mesh one by one using the above algorithm of cell refinement;

Step 3 Take the refined mesh as initial mesh and go to Step 1 until a satisfactory numerical velocity field is obtained or the threshold number T is reached.

In this paper, we subdivide a quadrilateral cell by connecting the mid-points of two opposite sides of a quadrilateral [1] and set $T = 2$, that is, we subdivide the cells on which one of the MC conditions is satisfied at most twice.

Accuracy Verifications by Comparison with Benchmarks

The accuracy is examined by using numerical velocity fields with the residuals less than 10^{-8} for both u and v. The initial mesh has a step size of 0.1 in both x and y directions. The initial velocity field is $u = v = 0$. The accuracy of the AMR method depends fully on the accuracy of the numerical velocity fields calculated by Navier2D. The profiles of u of the numerical velocity fields show the accuracies of the calculated fields (refer to Figs. 2, 3, 5, 6, 8, 9, 11, and 12). The refined meshes show the accuracy of the AMR method.

The Reynolds number is defined as $Re = \frac{UD}{\upsilon}$ where U is the inlet mean velocity or in other words two thirds of the maximum inlet horizontal component of the velocity field and the D is the hydraulic diameter of the inlet channel which is equivalent to twice the inlet channel height h [19]. However, as you will see, the Reynolds numbers Re are not same using the above two definitions for each of the cases considered in this section. Therefore, the Re in the following subsections are estimates. In this study, we make the maximum horizontal component of the numerical velocity fields at the step approximately 1.5 by choosing appropriate boundary condition at the inlet. We set different CFL numbers in Navier2D for different Reynolds numbers. The CFL condition is a necessary condition for convergence and stability of a numerical method. We choose suitable CFL numbers to obtain reliable numerical solutions.

$Re = 100$

Figs. 2 and 3 show the comparisons between the profile of the horizontal component u of the exact analytical velocity and the calculated ones on the initial and once refined meshes at the step. From these figures, we understand the differences between the exact Re and calculated ones. The difference between the profiles of analytical u and the calculated one on the initial mesh is smaller than that on the once refined mesh. However, the profile on the once refined mesh has better agreement with the profile generated using 500 uniform cells on the inlet

channel upstream of the step with length $20h$ and width h, and the analytical u profile as the inlet boundary condition (Figure 3 [19]). The u profiles for low Reynolds numbers are slightly different from the corresponding exact analytical profiles [19].

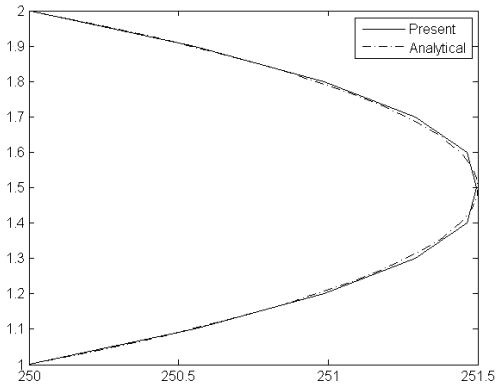

Figure 2. Comparison of the profiles of u at the step for $Re = 100$ between the current study and the analytical solutions on initial mesh

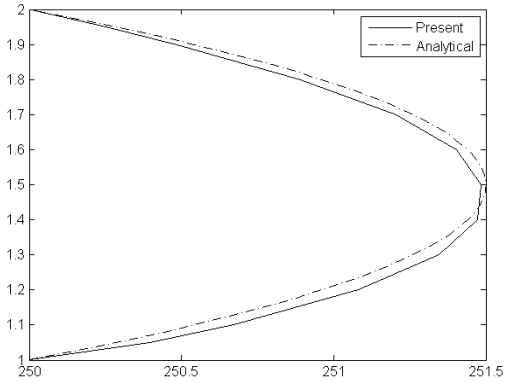

Figure 3. Comparison of the profiles of u at the step for $Re = 100$ between the current study and the analytical solutions on once refined mesh

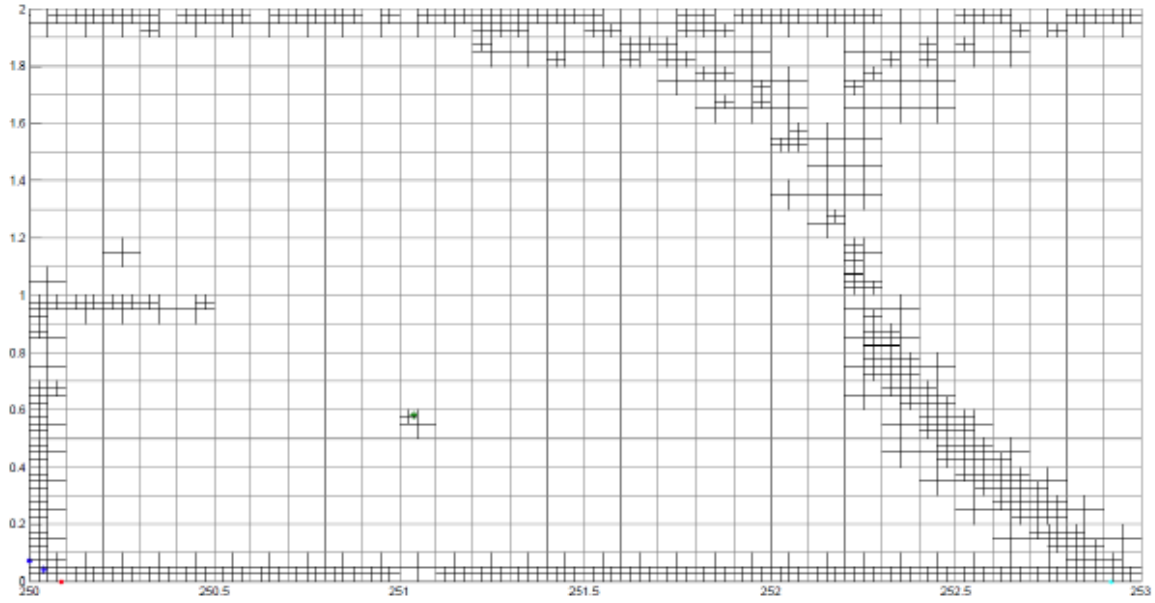

Figure 4. Twice refined mesh for $Re = 100$ with locations of detachment, reattachments and vortex centre

The once refined and twice refined meshes are shown in Figure 4. The locations of all detachment, reattachment and centers of vortices are held within the twice refined cells.

$Re = 200$

The u profiles for $Re = 200$ are shown in Figs. 5 and 6. They present similar patterns to those for $Re = 100$ in Figs. 2 and 3 but bigger differences between the analytical and calculated u profiles at the step for both cases.

The locations of all detachment, reattachment and centers of vortices are held within the twice refined cells as shown in Figure 7.

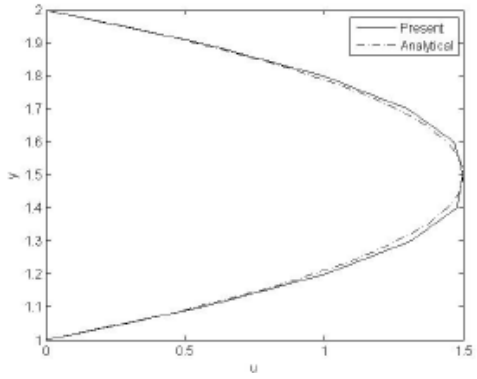

Figure 5. Comparison of the profiles of u at the step for $Re = 200$ between the current study and the analytical solutions on initial mesh

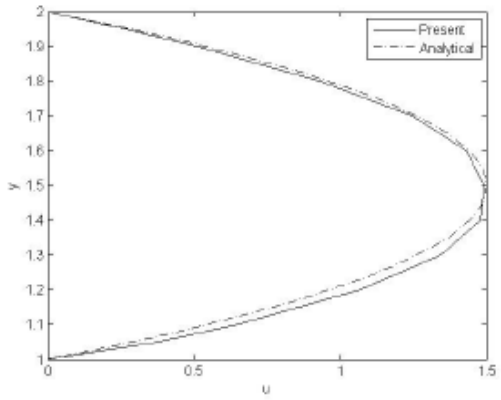

Figure 6. Comparison of the profiles of u at the step for $Re = 100$ between the current study and the analytical solutions on once refined mesh

$Re = 400$

The u profiles for $Re = 400$ are shown in Figs. 8 and 9. Once again, similar patterns to those for $Re = 100$ are obtained with even bigger differences between the analytical and calculated u profiles for both cases.

The locations of all detachment, reattachment and centres of vortices below the middle line of the channel and x_2 are held within the twice refined cells but the locations of x_3 and the centre of vortex x_2-x_3 are held within the once refined cells only as shown in Figure 10. Finer initial mesh or more accurate computational velocity field is required for $Re = 400$ from the u profiles.

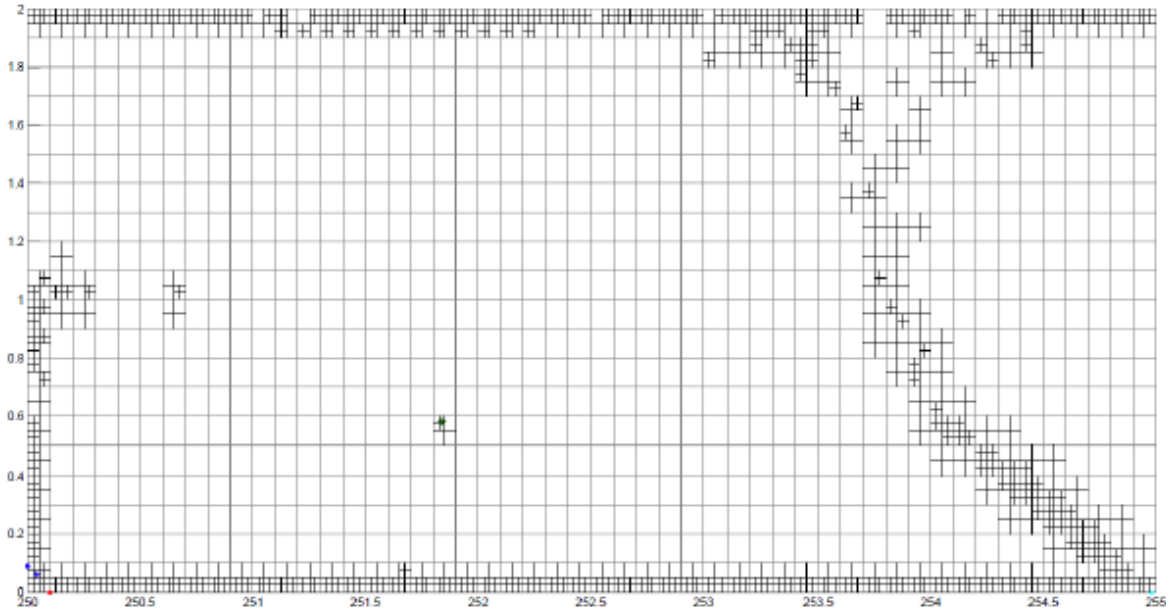

Figure 7. Twice refined mesh for $Re = 200$ with locations of detachment, reattachments and vortex centre

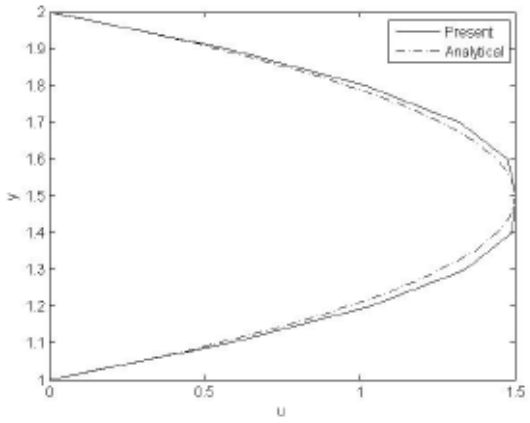

Figure 8. Comparison of the profiles of u at the step for $Re = 400$ between the current study and the analytical solutions on initial mesh

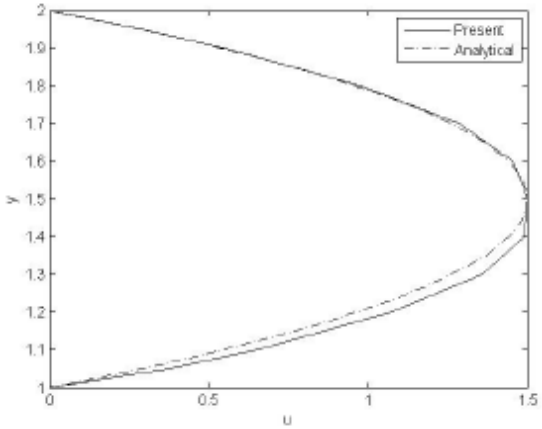

Figure 9. Comparison of the profiles of u at the step for $Re = 400$ between the current study and the analytical solutions on once refined mesh

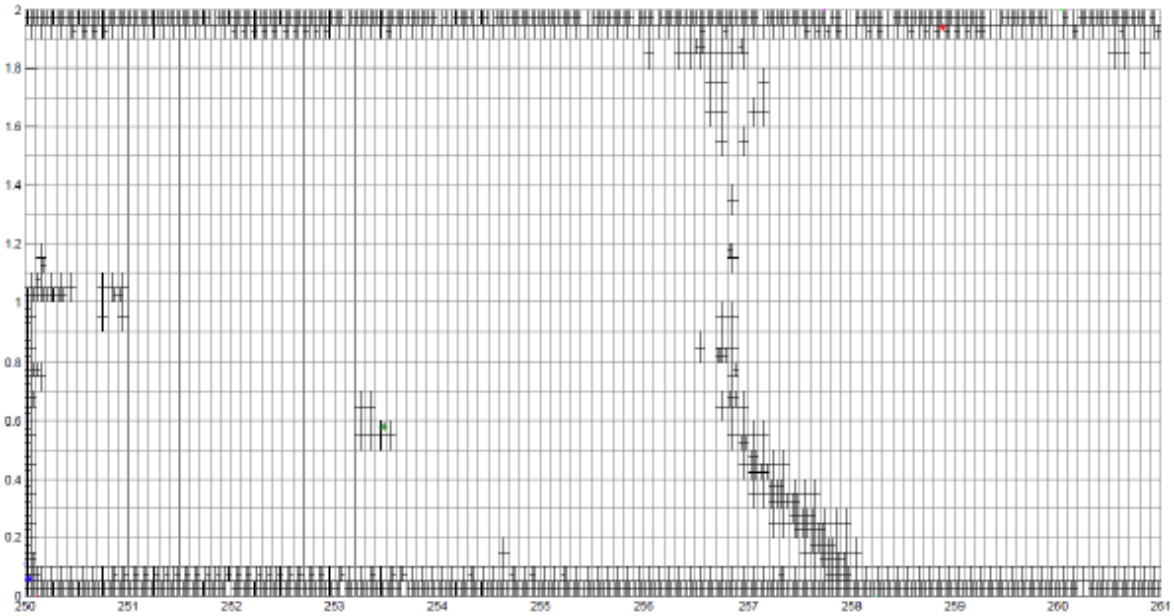

Figure 10. Twice refined mesh for $Re = 400$ with locations of detachment, reattachments and vortex centre

$Re = 800$

Figs. 11 and 12 show the largest differences between the analytical and calculated u profiles for all Reynolds numbers considered. The differences may be not acceptable in practice. Finer initial mesh or more accurate computational velocity field is required for better outcomes.

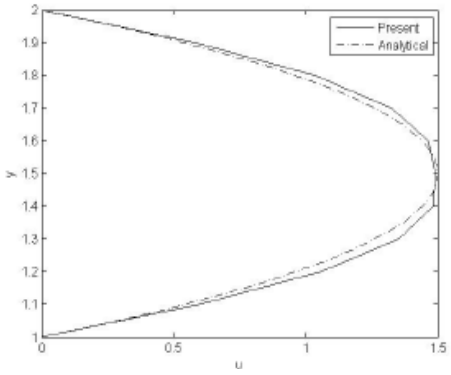

Figure 11. Comparison of the profiles of u at the step for $Re = 800$ between the current study and the analytical solutions on initial mesh

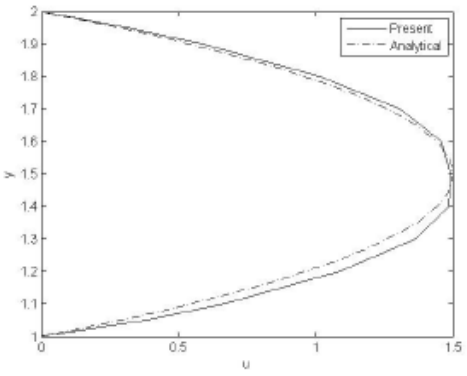

Figure 12. Comparison of the profiles of u at the step for $Re = 800$ between the current study and the analytical solutions on once refined mesh

The locations of y_0, x_1, and the centre of primary vortex are held within the twice refined cells but x_0 and center of vortex y_0-x_0 are held within the once refined cells as shown in Figure 13. The locations of x_2 and x_3 are held within the twice refined cells but the center of vortex x_2-x_3 is held within a cell without any refinements as shown in Figure 14.

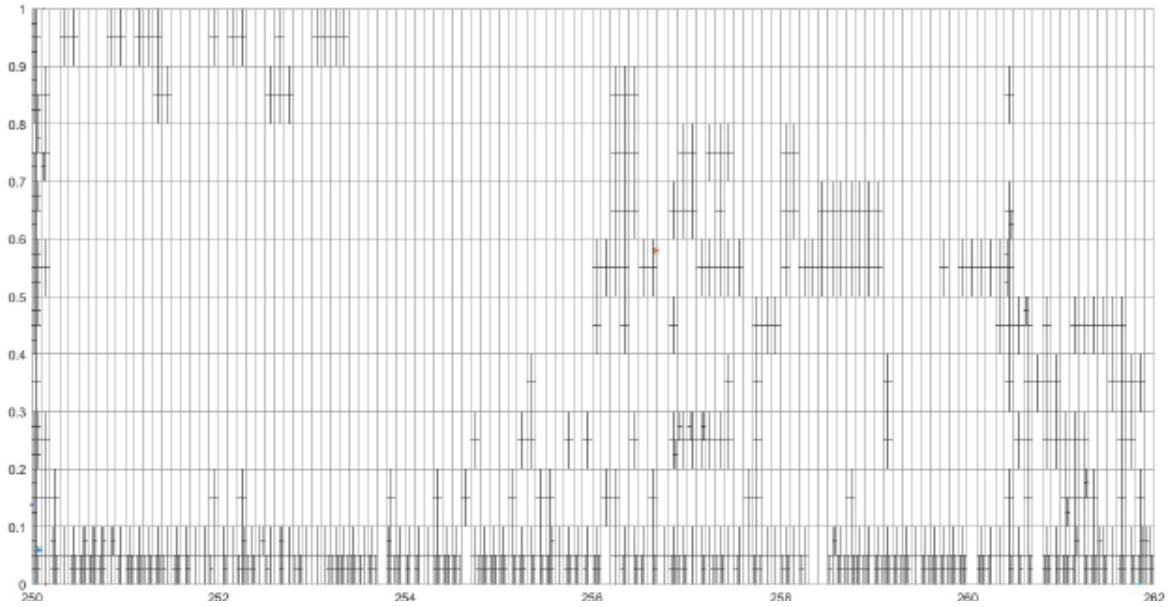

Figure 13. Twice refined mesh for $Re = 800$ with locations of detachment, reattachment and vortex centre for y in [0, 1]

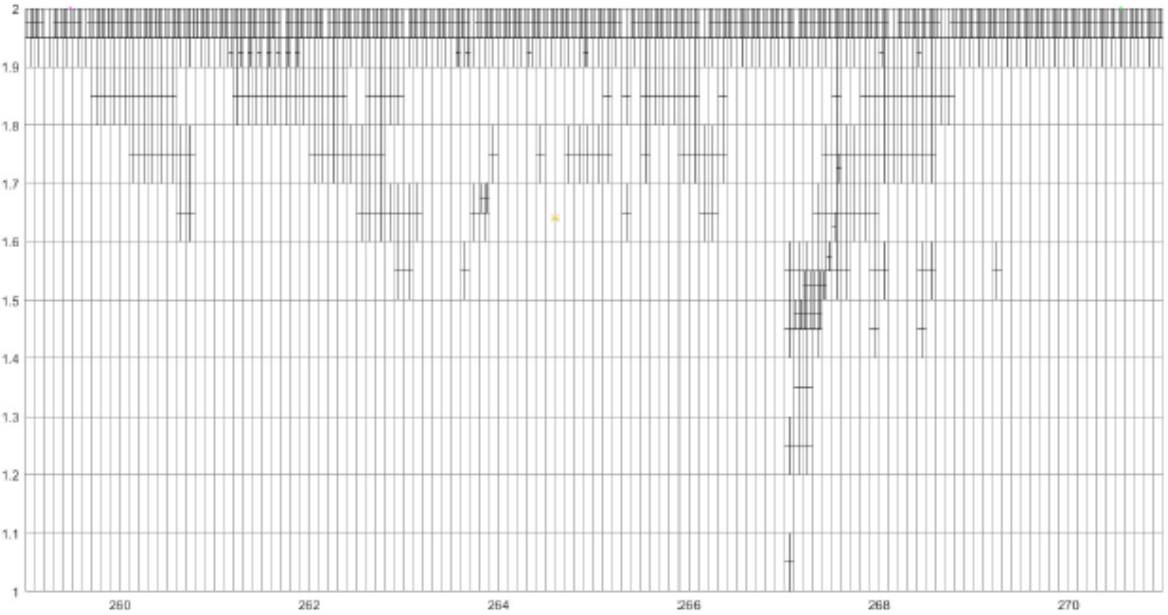

Figure 14. Twice refined mesh for $Re = 800$ with locations of detachment, reattachment and vortex centre for y in [1, 2]

Estimated Locations of the Centres of Vortices

Table 2 shows the coordinates of vortex centers from the benchmark [20] and the corresponding coordinates for $Re = 100$, 200, 400, and 800 calculated from the linearly interpolated velocity fields $\boldsymbol{V}_l$ on the initial and once refined meshes. The first row in the table are the

estimated centres using initial mesh, the second row are the estimated centers using the once refined mesh and the last row are benchmarks for each category. There are a number of singularities around point (13.8705, 1.6494) in the MATLAB outputs for vortex x_2-x_3 and case $Re = 800$ on the once refined mesh with one example illustrated in Table 2 below.

Table 2. Estimated locations of the centers of vortices

Vortex type	Reynolds numbers			
	Re = 100	Re = 200	Re = 400	Re = 800
y_0–x_0	-	-	-	-
	-	(0.0500, 0.0000)	(0.0525, 0.0587)	(0.0651, 0.0649)
	(0.04,0.04)	(0.04, 0.06)	(0.04, 0.06)	(0.08, 0.06)
x_0–x_1	(1.0404, 0.5759)	(1.8413,0.5885)	(3.4877,0.5927)	(6.6667,0.5875)
	(1.0466, 0.5731)	(1.8440,0.5824)	(3.5101, 0.5814)	(6.4437,0.5834)
	(1.04,0.58)	(1.84, 0.58)	(3.48, 0.58)	(6.68, 0.58)
x_2–x_3	-	-	-	(13.8743,1.6537)
	-	-	(8.5595, 1.9490)	(13.8705,1.6494)
	-	-	(8.88,1.94)	(14.60, 1.64)

Conclusions

We applied the AMR method twice to the initial meshes based on the numerical solutions of 2D backward facing step flow produced by Navier2D. The accuracy of the AMR method shown is sufficient for $Re = 100$ and 200, and is acceptable for $Re = 400$ and 800 based on the differences between the profiles of the horizontal component of the velocity fields at the step. The conclusion is that one setting for the domain, initial mesh and the residual error cannot achieve similar accurate numerical velocity fields for different Reynolds numbers. Therefore, the further research topics may include:

- Use longer lengths of upstream and downstream channels of the step for bigger Reynolds numbers.
- Use finer initial meshes when Reynolds number increases.
- Calculate more accurate numerical velocity fields when Reynolds number increases.

References

[1] Li, Z., and Wood, R. (2017) Accuracy verification of a 2D adaptive mesh refinement method for incompressible or steady flow, *J. Comput. Appl. Math.* **318**, 259--265.

[2] Li, Z. (2017) Computational complexity of the algoriithm for a 2D adaptive mesh refinement method using li-driven cavity flows, *Comput. Therm. Sci.* **9**, 395--403.

[3] Almgren, A., Bell, J., Colella, P., Howell, L. and Welcome, M. (1998) Conservative adaptive projection method for the variable density incompressible Navier--Stokes equations, *J. Comput. Phys.* **142**, 1--46.

[4] Lohner, R. (1987) An adaptive finite element scheme for transient problems in CFD, *Comput. Methods in Appl. Mech. Eng.* **61**, 323--338.

[5] Bell, J., Berger, B., Saltzman, J., and Welcome, M. (1994) Three dimensional adaptive mesh refinement for hyperbolic conservation laws, *SIAM J. Sci. Comput.* **15**, 127--138.

[6] Miller, K. and Miller, R. (1981) Moving finite elements, Part I, *SIAM J. Numer. Anal.* **18**, 1019--1032.

[7] Capon, P. and Jimack, P., An adaptive finite element method for the compressible Navier--Stokes equations, *Numerical Methods for Fluid Dynamics*, 1995, K. Morton and M. Baines, Eds, 327--333. Clarendon Press.

[8] Li, Z. (2008) An adaptive two-dimensional mesh refinement method based on the law of mass conservation, *J. Flow Visual. Image Process* **15**, 17--33.

[9] Li, Z. (2007) An adaptive three-dimensional mesh refinement method based on the law of mass conservation, *J. Flow Visual. Image Process* **14**, 375--395.

[10] Ye, Y. and Others (1986) Theory of Limit Cycles, Providence, Rhode Island: American Mathematical Society Press.

[11] Erturk, E., Corke, T.C. and Gökcöl (2005) Numerical solutions of 2-D steady incompressible driven cavity flow at high Reynolds numbers, *Int. J. Numer. Methods Fluids* **48**, 747--774.
[12] Li, Z. (2006) An adaptive streamline tracking method for two-dimensional CFD velocity fields based on the law of mass conservation, *J. Flow Visual. Image Process.* **13**, 1--14.
[13] Li, Z. (2006) An adaptive streamline tracking method for three-dimensional CFD velocity fields based on the law of mass conservation, *J. Flow Visual. Image Process.* **13**, 359--376.
[14] Lal, R. and Li, Z. (2015) Sensitivity analysis of a mesh refinement method using the numerical solutions of 2-D steady incompressible driven cavity flow, *J. Math. Chem.* **53**, 844--867.
[15] Faure, S., Laminie, J. and Temam, R. (2008) Colocated finite volume schemes for fluid flows, *Commun. Comput. Phys.* **4**, 1--25.
[16] Li, Z. (2014) Accuracy analysis of a mesh refinement method using benchmarks of 2-D lid-driven cavity flows and finer meshes, *J. Math. Chem.* **52**, 1156--1170.
[17] Armaly, B., Durst, F., Pereir, J. and Schönung, B. (1983) Experimental and theoretical investigation of backward-facing step flow, *J. Fluid Mech*.**127**, 473--496.
[18] Li, Z. and Wood, R. (2015) Accuracy analysis of an adaptive mesh refinement method using benchmarks of 2-D steady incompressible lid-driven cavity flows and coarser meshes, *J. Comput. Appl. Math*. **275**, 262--271.
[19] Li, Z. (2017) Analysis of 2D unsteady flow past a square cylinder at low Reynolds numbers with CFD and a mesh refinement method, *WSEAS Trans. on Fluid Mech*. **12**, 150--157.
[20] Erturk, E. (2008) Numerical solutions of 2-D steady incompressible flow over a backward-facing step, Part I: High Reynolds number solutions, *Comput. Fluids* **37**, 633--655.
[21] Engwirda, D. (2006) Navier-Stokes Solver (Navier2d), MATLAB Central File Exchange. Last accessed May 2006.
[22] Li, Z. and Mallinson, G., Simplification of an existing mass conservative streamline tracking method for two-dimensional CFD velocity fields, *GIS and Remote Sensing in Hydrology, Water Resources and Environment*, 2004, Y. Chen, K. Takara, Cluckies I, F.H. DS., Eds, 269—275, IAHS Press, Wallingford, UK.
[23] Li, Z. (2002) A mass conservative streamline tracking method for two-dimensional CFD velocity fields, *J. Flow Visual. Image Process.* **9**, 75--87.